Macromolecules

Cite This: Macromolecules 2018, 51, 8605−8610

Article

pubs.acs.org/Macromolecules

Nonlinear Viscoelastic Modeling of Adhesive Failure for Polyacrylate Pressure-Sensitive Adhesives

Julien Chopin,*[,†,‡] Richard Villey,[§] David Yarusso,[∥] Etienne Barthel,[†] Costantino Creton,[†] and Matteo Ciccotti*[,†]

[†]Laboratoire Sciences et Ingénierie de la Matière Molle, PSL Research University, UPMC Univ Paris 06, ESPCI Paris, CNRS, 10 rue Vauquelin, Cedex 05 75231 Paris, France

[‡]Instituto de Física, Universidade Federal da Bahia, Campus Universitário de Ondina, rua Barão de Jeremoabo, BA 40210-340, Brazil

[§]Saint-Gobain Glass France, Chantereine R&D Center, 1 rue de Montluçon - BP 40103, Cedex 60777 Thourotte, France

[∥]3M Center, 3M Company, 230-1D-15, St. Paul, Minnesota 55144-1000, United States

ABSTRACT: We investigate experimentally the adherence energy Γ of model polyacrylate pressure-sensitive adhesives (PSAs) with combined large strain rheological measurements in uniaxial extension and an instrumented peel test. We develop a nonlinear model for such a peel test which captures the dependence of $\Gamma(V)$ with peeling rate V, revealing the key role played by the extensional rheology. Our model explains in particular why traditional linear viscoelastic approaches correctly predict the slope of $\Gamma(V)$ curves for sufficiently elastic PSAs characterized by a simple rate-independent debonding criterion. However, for more viscoelastic adhesives, we identified a more complex rate-dependent debonding criterion yielding a significant modification of the $\Gamma(V)$ curves, an effect that has been largely overlooked so far. This investigation opens the way toward the understanding of fibrils debonding, which is the main missing block to predict the adherence of PSAs.

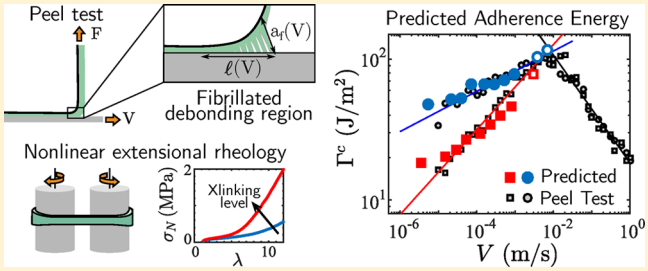

INTRODUCTION

It is a very well-known result that during the peeling of a typical viscoelastic PSA from a solid substrate, the measured adherence energy Γ (the energy required to peel a unit tape area) is several orders of magnitude above the value given by the thermodynamic work of adhesion between the adhesive and the substrate. Moreover, in the slow steady state regime, Γ is very dependent on the temperature T and peeling rate V. It has long been observed that for viscoelastic adhesives the adherence curves $\Gamma(V,T)$ can be collapsed to a single master curve $\Gamma(a_T V,T^{\mathrm{ref}})$ at a reference temperature T^{ref} by renormalizing the velocity axis by the same shift factor a_T that is used for the time−temperature superposition (TTS) of the linear rheological measurements.[1−5] This has suggested that linear viscoelasticity should be used to quantitatively model the adherence energy $\Gamma(V,T)$.

Various linear viscoelastic models have since been developed based on a perturbation of the linear elastic fracture mechanics (LEFM) crack tip singular fields.[6−11] These models predict a fracture energy in the separable form $\Gamma(V,T) = \Gamma_0(1 + \Phi(a_T V))$,[12,13] where Γ_0 is an intrinsic adhesion energy and $\Phi(a_T V)$ is a factor accounting for the linear viscoelastic losses. However, most attempts to quantitatively check these predictions experimentally for soft adhesives and rubbers have up to now failed.[11,14,15] Even an important protagonist of this domain such as Gent[14] has pointed out the intrinsic limitation of these theories to describe experimental data since they would predict a process zone of unphysical subatomic size.

When considering soft PSAs, the elastoadhesive length scale Γ/E, where large strains are present around the crack tip,[16,17] is comfortably larger than the typical 20 μm thickness of the adhesive layer used for tapes.[18] Because the LEFM approach relies on a clear separability of scales between the crack tip singular field and the bulk sample deformation, it cannot be applied to PSAs in most practical situations. Alternative modeling approaches have been developed to account for the strong confinement of the material based on a linear viscoelastic foundation following the pioneering work of Kaelble.[3,19,20] But the experimentally observed development of a dense array of highly stretched fibrils in the debonding region is at odds with this linear approach.[21−24] The role played by the fibrillated region in the overall dissipation was pointed out by several polymer rheologists,[2,25,26] but most experimental investigations were made on non-cross-linked fluidlike adhesives, where failure occurs either cohesively in the fibrils or without fibrillation at all. Such viscoelastic fluids even if able to strain harden in extension are not representative of

Received: June 27, 2018
Revised: September 14, 2018
Published: October 22, 2018

DOI: 10.1021/acs.macromol.8b01374
Macromolecules 2018, 51, 8605−8610

the lightly cross-linked polymers used for PSA that form an extended fibrillar zone that cleanly debonds from the surface of the substrate. Thus, the respective roles played in the peeling process by the linear, small strain dissipation controlled by the monomer friction coefficient and by the nonlinear extensional rheology, where strain hardening due to chain architecture is important, remain elusive. The same conclusion has been reached with other classically used adhesive tests such as the probe-tack test.[29,30]

In a previous investigation,[18] we specifically studied a series of model lightly cross-linked polyacrylate adhesives with different behaviors in extensional rheology but nearly identical small strain dissipation at the strain rates relevant for peeling. We showed from steady state peeling experiments that a more pronounced strain hardening caused an overall decrease of the peeling force and a stronger dependence with peeling rate, which cannot be explained by any model based on linear rheology (see Figure 5a). In parallel, a quantitative characterization of the debonding region by optical microscopy revealed that the fibrils always detached cleanly from the substrate after a stretch larger than 500%, which diminished with peeling velocity, confirming that nonlinear material properties matter here. Similar experiments were later performed and reported by Barrios.[31] Moreover, we found that a more pronounced strain stiffening causes the maximum fibril extension before detachment to decrease and to become less sensitive to the peeling rate.[18]

In this paper, we provide the first quantitative physically based model connecting nonlinear extensional rheological properties of model cross-linked PSAs with the adherence curves obtained in peel tests. We reconcile the TTS principle observed in the adherence curve and nonlinear deformation in the adhesive. Our results reveal complex debonding criteria, which unambiguously demonstrate the nontrivial role played by polymer chain architecture and hence nonlinear rheology in determining the $\Gamma(V)$ curves.

EXPERIMENTAL SECTION

The model PSAs were synthesized by free radical polymerization in solution from 85 wt % 2-ethylhexyl acrylate (EHA), 10 wt % methyl acrylate (MA), and 5 wt % acrylic acid (AA). 0.2 or 0.4 wt % aluminum acetyl acetonate relative to monomer was added after synthesis to provide two levels of cross-linking (labeled A and B) to the adhesive layer which were coated between two silicone release liners.

The linear viscoelastic characterization of the polymers was performed with an Anton-Paar rheometer (MCR-301) using a standard parallel plate geometry (Figure 1a). The storage $G'(\omega,T)$ and loss $G''(\omega,T)$ shear moduli were measured at pulsation ω in the range 2×10^{-1} to 60 rad/s. Pulsation sweeps were performed for temperatures T in the range −40 to 120 °C. The maximum applied shear strain is $\gamma = 2 \times 10^{-2}$.

The nonlinear rheological properties are obtained by extensional rheology measurements using the Sentmanat extensional rheometer (SER, see Figure 1b),[32] adapted on the same MCR-301 rheometer. A slab of the polymer of width $W = 5$ mm and thickness $e = 600$ μm is brought in contact with the cylinders. The stickiness of the materials guarantees a no slip condition at the interface. The cylinders were rotated at a constant angular velocity, resulting in a constant true strain rate $\dot{\varepsilon}$ in the range 10^{-2}–4 s^{-1}. The temperature was varied in the range 0–40 °C. The cross-section area of the deformed slab is given by $A(t) = eW \exp(-\dot{\varepsilon}t)$. True strain and stress are given by $\varepsilon(t) = \dot{\varepsilon}t$ and $\sigma(t) = F(t)/A(t)$, respectively, where t is time and F is the measured force acting on the slab. Nominal stress is $\sigma_N = \sigma/\lambda$, where $\lambda = \exp(\varepsilon)$ is the stretch.

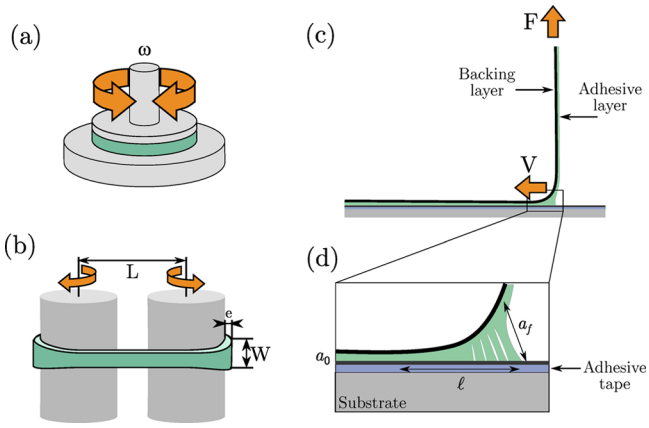

Figure 1. Schematics of experimental setups. (a) Linear shear storage $G'(\omega)$ and loss $G''(\omega)$ moduli of the adhesives are measured by dynamical mechanical analysis in a parallel plate geometry at imposed pulsation ω. (b) Nonlinear rheological properties are measured with the Sentmanat extensional rheometer which measures the applied force on an adhesive slab under uniaxial stretching condition at constant strain rate. (c) Instrumented peeling tests are performed with the same adhesives coated on a PET backing which is peeled by a vertical force F and peeling rate V. (d) Sketch of the fibrillar debonding region where l is the lateral size and a_f the maximal fibril size before detachment from the substrate. A commercial adhesive tape is bonded to a glass or aluminum substrate to ensure clean peeling and repeatable results.

Finally, instrumented peel tests were performed at a 90° angle by applying a force F at a peeling rate V (Figure 1c). As detailed elsewhere,[18] the peeling occurred at either imposed load or imposed velocity, allowing us to explore a large range of peeling rates from 1 μm/s to 4 m/s. The same model adhesives were coated on a 38 μm thick PET film. The adhesive layer thickness $a_0 = 19$ μm. All adhesive tapes were carefully bonded to the release side of a commercially available adhesive tape which is itself bonded to a microscope glass slide for small and intermediate peeling rates and long aluminum profiles for higher peeling rates. This protocol ensures clean peeling and repeatable results. Because the PET backing layer is much stiffer than the adhesive, the energy release rate $\mathcal{G}$ in this geometry is given by

$$\mathcal{G} = \frac{F}{b} \tag{1}$$

where $b = 20$ mm is the tape width. In steady state, an energy balance yields $\mathcal{G} = \Gamma(V)$. In addition, the experimental setup was equipped with a lateral optical microscope allowing to image the structure of the debonding region with a micrometric resolution (Figure 1d).

Thus, the peeling test was performed to characterize the structure of the debonding region while measuring macroscopically the adherence curves $\Gamma(V)$. Insights into viscoelastic dissipative processes occurring in the debonding region have been obtained from linear and nonlinear rheological measurements in controlled and imposed geometries. In the remainder of the paper, we will present in turn the results obtained from each experimental setup. We will finally present our model, developed to predict the macroscopic adherence curves of lightly cross-linked PSA from bulk rheological properties and detailed knowledge of the structure of the debonding region.

RESULTS

In Figure 2, we present the results obtained from linear rheological measurements. We plot the rescaled storage shear modulus $b_T G'$ in Figure 2a and the rescaled loss modulus $b_T G''$ in Figure 2b as a function of the rescaled pulsation $a_T\omega$ at a reference temperature $T^{ref} = 296$ K. The horizontal shift factor

DOI: 10.1021/acs.macromol.8b01374
Macromolecules 2018, 51, 8605–8610

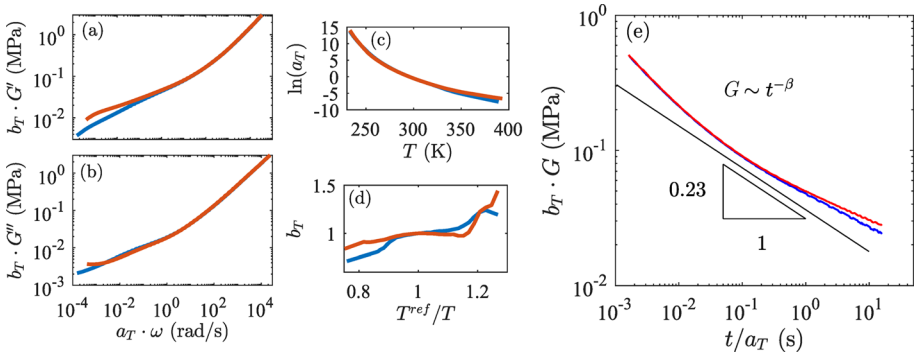

Figure 2. (a) Rescaled storage shear modulus $b_T G'$ and (b) loss shear modulus $b_T G''$ for both polymers, which present an identical linear rheological response for $a_T\omega > 10^{-1}$ rad/s. The reference temperature is $T^{ref} = 296$ K. (c) Horizontal shift factor a_T and (d) vertical shift factor b_T as a function of temperature T for both polymers. (e) Rescaled relaxation shear modulus $b_T G(t)$. Its time dependence is roughly approximated by $G \sim t^{-\beta}$ with $\beta = 0.23$.

a_T and vertical shift factor b_T are shown in Figures 2c and 2d, respectively. Over the range of temperatures and rates used in the peel tests and extensional rheology, $b_T \approx 1$ within 10% error. The dependence of the horizontal shift factor with temperature can be captured using the Williams–Landel–Ferry model:

$$\ln a_T = -C_1 \frac{T - T^{ref}}{C_2 + T - T^{ref}} \quad (2)$$

with $T^{ref} = 296$ K. A fit of the experimental data over the entire temperature range gives for polymer A $C_1 = 19.5$ and $C_2 = 154.4$ K and for polymer B $C_1 = 12.6$ and $C_2 = 118.6$ K. In Figure 2e, we calculate the relaxation shear modulus $G(t)$ at temperature T^{ref} using the Cox–Merz rule,[27] yielding $G(t = \omega^{-1}) \simeq \sqrt{G'^2(\omega) + G''^2(\omega)}$. This can be roughly approximated by a power law $G \sim t^{-\beta}$ with $\beta = 0.23$ in the relevant range for peel. We can readily see that the level of cross-linking does not significantly affect the linear rheological response of the material or the shift factors.

Typical nonlinear extensional curves $\sigma_N(\lambda)$ are shown in Figure 3a–c for independent changes of the cross-linking level, strain rate, and temperature. In all cases, after a linear regime at $\lambda \sim 1$, we observe a softening followed by a strain hardening, as expected for PSAs.[33] Figure 3a shows that when increasing the level of cross-linking (at $\dot{\varepsilon} = 1$ s^{-1} and $T = 20$ °C), the curves are first superimposed in the linear regime as expected and then significantly depart from it at $\lambda \approx 3$–4 while still in the softening regime. The typical stretch λ_c for the onset of strain hardening is $\lambda_c = 7$ (respectively 5) for polymer A (respectively B). Figure 3d shows that the variation of σ_N with $\dot{\varepsilon}$ and T can be captured by a single prefactor $\mathcal{A}(\dot{\varepsilon}, T)$ allowing to collapse all the curves on a reference master curve, where $\mathcal{A}(\dot{\varepsilon}^{ref} = 1$ s^{-1}, $T^{ref} = 296$ K$) = 1$. The stress curves can then be written in a separable form $\sigma_N(\lambda, \dot{\varepsilon}, T) = \mathcal{A}(\dot{\varepsilon}, T)\sigma_N^{ref}(\lambda)$, where $\sigma_N^{ref}(\lambda)$ only depends on the stretch λ and on the cross-linking level. This separability is less obvious for the polymer A with a lower level of cross-linking, especially for low T and large λ where nonlinear relaxation processes typical of viscoelastic fluids are active.[34] However, it provides a good description of the nonlinear rheology in the domain of stretch experienced by fibrils before debonding in peeling.

In the inset of Figure 4, the prefactor $\mathcal{A}$ for polymers A and B is plotted on a log–log scale as a function of $\dot{\varepsilon}$ for the range of temperatures for which we have performed nonlinear tests.

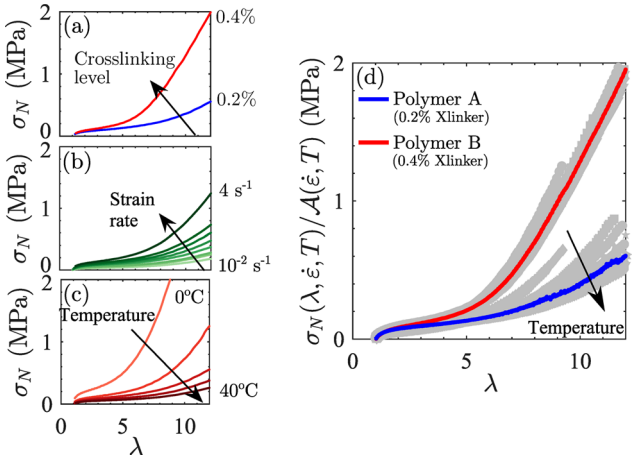

Figure 3. (a–c) Nonlinear extensional curves representing the nominal stress σ_N versus stretch λ, varying (a) concentration of cross-linker level, (b) strain rate $\dot{\varepsilon}$, and (c) temperature T. All the curves show a softening regime followed by a strain hardening. Higher concentrations of cross-linker induce stiffening at large λ but make no observable difference at small λ. (d) All the rheological curves collapse on a master curve when rescaled by a single paremeter $\mathcal{A}(\dot{\varepsilon}, T)$ independent of λ.

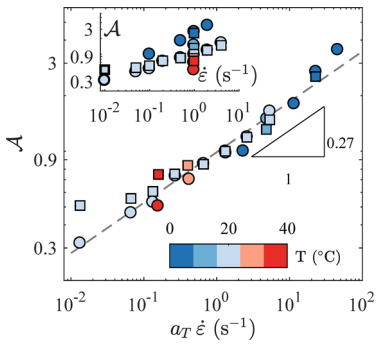

Figure 4. Rescaling factor $\mathcal{A}$ for both polymers is obtained from a fitting procedure over the entire range of strain rates for various temperatures in the range 0–40 °C (color bar). $\mathcal{A}(\dot{\varepsilon}, T)$ depends on both $\dot{\varepsilon}$ and T (inset: raw data) but can be collapsed to $\mathcal{A} \sim (a_T\dot{\varepsilon})^{0.27}$ when using the same shift factor a_T measured from the linear viscoelastic behavior.

In the main graphic of Figure 4, we show that the data can be collapsed onto a master curve when plotted against $a_T\dot{\varepsilon}$ where

DOI: 10.1021/acs.macromol.8b01374
Macromolecules 2018, 51, 8605–8610

a_T is the shift factor determined from linear rheology. Remarkably, the linear and nonlinear rheology are thus found to share the same TTS. Moreover, for both polymers, we find that $\mathcal{A} \sim (a_T\dot{\varepsilon})^{0.27}$ for $\dot{\varepsilon} > 10^{-2}$ s^{-1}. Deviations are observed at smaller $\dot{\varepsilon}$, but as it will be shown below, this occurs outside the range of strain rates experienced by the fibrils during our peeling tests. By construction, the same prefactor $\mathcal{A}$ can be used to rescale the true stress curves $\sigma(\varepsilon)$, yielding

$$\sigma(\varepsilon, \dot{\varepsilon}, T) = \mathcal{A}(a_T\dot{\varepsilon})\sigma^{\mathrm{ref}}(\varepsilon) \tag{3}$$

which is compatible with a Rivlin−Sawyers type of nonlinear constitutive law.[35] Because eq 3 is also valid in the small strain regime where we have $\sigma \sim G(t)\varepsilon(t)$, we obtain that $\mathcal{A}(a_T\dot{\varepsilon}) \sim G(a_T\dot{\varepsilon}) \sim (a_T\dot{\varepsilon})^{\beta}$ where we have used the Cox−Merz rule ($\dot{\varepsilon} \sim \omega \sim 1/t$).[27] The exponent $\beta = 0.23$ measured by linear rheology (cf. Figure 2e) is found to be in reasonable agreement with the 0.27 exponent obtained for nonlinear rheology. This strongly indicates that most of the rate and temperature dependence of both polymers is encapsulated in a single linear rheology function $\mathcal{A}$, in the range relevant for the measured peeling curves.

Next, we focus on the characterization of the fibrillated debonding region during steady state peeling using an instrumented peel test[18,36] at a 90° angle and T = 23 °C. From images of the fibrillated debonding region, we measured both the lateral size l of the fibrillar debonding region and the maximum fibril length a_f at debonding (see Figure 1d). In Figure 5a, we reproduced the adherence curves as a function of

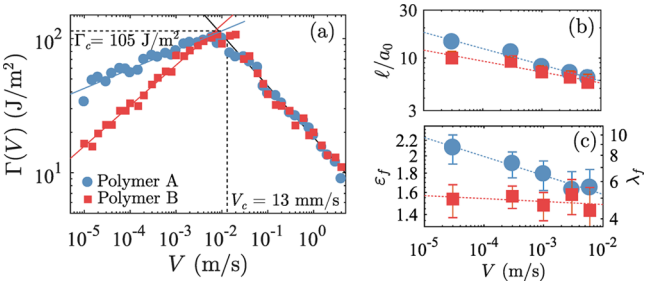

Figure 5. (a) Measured adherence energy $\Gamma(V)$ for polymers A and B. Above a characteristic peeling rate V_c, a stick−slip instability develops for both polymers. Data from Villey et al.[18] (b) Reduced lateral size decreases with speed as $l/a_0 \sim V^{-p}$ with p = 0.16 (respectively p = 0.10) for polymer A (respectively B). (c) Final strain $\varepsilon_f = \ln(\lambda_f)$ is described by $\varepsilon_f \sim V^{-q}$ where q = 0.05 (respectively q = 0.007) for polymer A (respectively B).

the peeling rate for polymers A and B from data collected in Villey et al.[18] As mentioned in the Introduction, polymer B which has a more pronounced strain hardening presents a lower adherence than polymer A but a stronger dependence with the peeling rate. The adherence curves for the two polymers are distinct until reaching a critical velocity V_c = 13 mm/s, above which they exhibit an identical trend characterized by a negative slope. The region $V > V_c$ corresponds to an unsteady peeling caused by a stick−slip instability.[37] However, in the present paper, we focus on the steady-state peeling regime with a well-defined peeling rate. In this regime, the normalized lateral size l/a_0 shown in Figure 5b is found to decrease as a power law $l \sim V^{-p}$ with an exponent $p \simeq 0.13$ weakly dependent on the cross-linking level. The characteristic time scale for stretching the fibrils $t_f = l/V$ is in the range 0.01−20 s—a regime where linear rheological measurements show no difference between polymers A and B (see Figure 2). The maximal fibril stretch $\lambda_f = a_f/a_0$ is plotted in Figure 5c. For both polymers, the fibrils are stretched outside the regime of linear viscoelasticity and reach the strain hardening regime before debonding from the substrate (see Figure 3). Therefore, we expect that material nonlinearities are also a key ingredient at smaller scale to model the failure mechanism of fibrils. The relation between the level of cross-linking and the maximal fibril stretch is however nontrivial. For polymer B, λ_f is roughly independent of the peeling rate and $\lambda_f \approx 5$. But for polymer A, we observe not only an overall larger λ_f but also a clear rate dependency. A fit of the data with a power law yields $\varepsilon_f = \ln(\lambda_f) \sim V^{-q}$ with q = 0.05 (respectively q = 0.007) for polymer A (respectively B). The fact that the effect of the level of cross-linking is more pronounced at a smaller peel rate is rather counterintuitive. Indeed, it is generally believed that the models of adhesion based on the assumption of linear viscoelasticity work best at smaller peel rates. This point will be clarified in the discussion of our model. Furthermore, we evaluate the average strain rate $\dot{\varepsilon}_a$ experienced by a fibril as $\dot{\varepsilon}_a \approx \varepsilon_f V/l \propto V^{1+m}$ where $m = p - q \ll 1$. For the measured peeling rates in the range 10^{-5}−10^{-2} m/s, the equivalent strain rate is in the range 5×10^{-2}−10^2 s^{-1} which is overlapped by the rheological measurements.

We are now in a position to propose a model to predict the adherence energy by combining the nonlinear material behavior and the measured characteristics of the fibrillated debonding region. Because the cavitation of the adhesive locally relaxes the effect of confinement,[38] we initially make the assumption that the large stretch of the fibrils can be treated as uniaxial. The adherence energy can thus be modeled as

$$\Gamma^c(V) = ka_0 \int_0^{\varepsilon_f(\dot{\varepsilon}_a)} \sigma(\varepsilon', \dot{\varepsilon}_a)\, \mathrm{d}\varepsilon' \tag{4}$$

where $\sigma(\varepsilon,\dot{\varepsilon}_a)$ is provided by the elongational measurements corresponding to the average strain rate $\dot{\varepsilon}_a$ and k is an adjustable factor compensating the crude approximation of uniaxial extension of fibrils, while the more complex fibril drawing condition will be investigated in future work. In the present implementation $\varepsilon_f(V)$ and $l(V)$ are measured quantities, since a model able to capture their functional dependence with the peeling speed has yet to be developed. The linear dependence of the adherence energy on the adhesive layer thickness has been demonstrated in previous experimental and theoretical studies.[28,39]

In Figure 6, we replot the $\sigma(\varepsilon,\dot{\varepsilon})$ curves for polymers A and B in terms of true stress and strain varying the strain rate at T = 20 °C, unless otherwise stated in the caption. The area under the curves is proportional to Γ^c/a_0 by the factor k. In Figure 7, we plot the model prediction Γ^c as a function of the peeling rate V according to eq 4, along with the steady state peeling data from our previous work.[18] The two data sets are in good agreement if the value of the peel prediction is multiplied by a dimensionless prefactor k = 5, demonstrating that eq 4 captures the clear difference in the adherence energy curves $\Gamma(V)$ between polymers A and B in terms of both relative values and slope, while a model based on linear rheology alone cannot explain this difference. The dimensionless prefactor k can be interpreted as the sign that the fiber drawing process from the bulk adhesive layer is affected by a higher stress triaxiality than uniaxial extension tests, which will be the focus of further investigation.

DOI: 10.1021/acs.macromol.8b01374
Macromolecules 2018, 51, 8605−8610

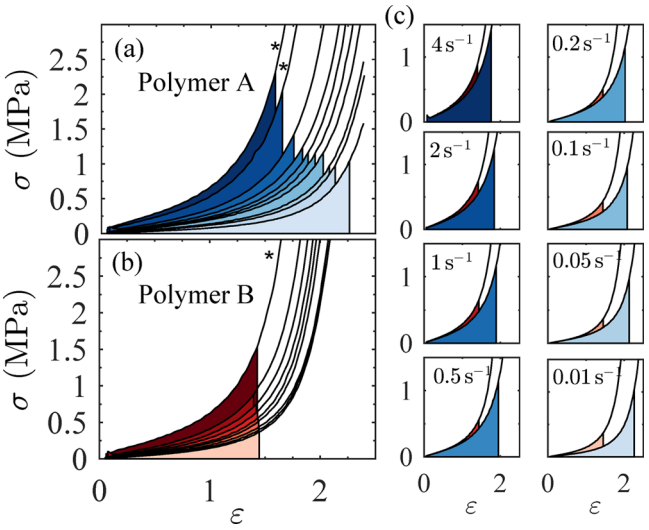

Figure 6. Evolution of the dissipated energy (proportional to the shaded areas) with $a_T\dot{\varepsilon}$ (shifted at a common temperature T = 20 °C) for (a) polymer A and (b) polymer B. Upper bounds for the integral $\varepsilon_f = \ln \lambda_f$ are obtained from data given in Figure 5c. Curves with a star label are measured at 0 °C and rescaled. (c) Comparison of the stress−strain curves and debonding criteria for polymers A and B for the same $\dot{\varepsilon}$ at T = 20 °C.

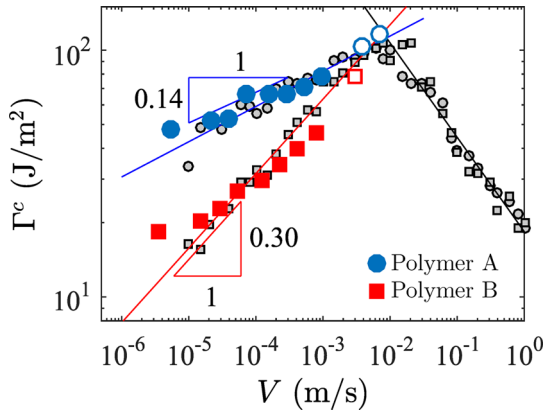

Figure 7. Calculated adherence curves Γ^c given by eq 4 (large blue and red symbols) superposed with peeling data from Villey et al.[18] (small gray symbols), already shown in Figure 5a. Using a numerical prefactor k = 5, quantitative agreement is obtained. Empty symbols are calculated from measurements taken at 0 °C.

The direct experimental access to the model parameters provides interesting insights into the physical mechanisms at the origin of the adherence curves in peeling. When focusing on the fibril debonding data in Figure 6a, we clearly see that the debonding criterion cannot be simply expressed in terms of a critical stress or strain.[26,40] However, for the more cross-linked polymer B, the debonding criterion is closer to a critical strain condition. In Figure 6c, we compare the stress curves for polymers A and B at specific values of $\dot{\varepsilon}$. We observe that although the stress level for B is always higher than for A, the overall dissipation, hence Γ^c, is larger for A due to the larger values of ε_f. Moreover, the observation that the two polymers present a different rate dependence of ε_f with $\dot{\varepsilon}$ explains why at higher $\dot{\varepsilon}$ the peeling energy Γ^c for both polymers tends to get closer. Therefore, we demonstrate that both the increase in the stress level with $\dot{\varepsilon}$ and the decrease of ε_f are crucial to determine the general trend of $\Gamma^c(V)$, making it difficult to derive *a priori* predictions unless we identify a sound fibril debonding criterion.

We can now discuss the link between our model and previous linear models. Taking advantage of the separability between strain rate dependence and strain dependence observed for our polymers (see eq 3), eq 4 can be further simplified as

$$\Gamma^c(V) \propto \mathcal{A}(a_T\dot{\varepsilon}_a)\int_0^{\varepsilon_f(\dot{\varepsilon}_a)} \sigma^{ref}(\varepsilon)\, d\varepsilon \tag{5}$$

which more clearly reveals two contributions to $\Gamma^c(V)$: (1) a rate-dependent linear viscoelastic factor and (2) a nonlinear factor whose rate dependence originates from the debonding criterion. If we first consider polymer B alone, for which ε_f is essentially rate independent, the dependence on rate of the adherence curve $\Gamma^c(V) \propto V^n$ is completely determined by linear rheology and the power law exponent of n = 0.30 is quite close to the measured values of $\beta \sim 0.23-0.27$. This result can explain why several authors have previously observed the TTS superposition for the adherence curves and the correlations between the n and β exponents. However, when considering the behavior of polymer A, which has a less elastic character, the maximum fibril stretch at debonding ε_f becomes significantly dependent on the peel rate, and the competition between the increase in stress and the decrease in maximum stretch affects the $\Gamma^c(V)$ curve in a deeply nonlinear manner. It is worth noting that even in the low speed regime, where LEFM-based approaches are generally considered to be more appropriate, extremely soft materials, such as polymer A, are shown to be stretched increasingly outside their linear viscoelastic regime, thus precluding the use of linear models.

CONCLUSION

We have shown that the peel force of model soft viscoelastic PSAs can be quantitatively modeled for a range of strain rates with a single adjustable dimensionless prefactor based on experimentally measured values of the maximum stretch in the fibrils at the detachment point. For more cross-linked adhesives the stress can be separated into the product of a strain-dependent term that characterizes the strain softening and hardening behavior of the adhesive and a strain rate-dependent term that characterizes the molecular friction and is dependent on the glass transition temperature of the adhesive. However, for weakly cross-linked adhesives the two factors are no longer easily separable, and the functional form of the strain hardening depends on the strain rate, especially for very large strains.

A detailed modeling of both the relevant stress triaxiality during the fibril drawing process and of the fibril debonding criterion is certainly the next step, but we believe that the present model provides a clear understanding of the ingredients needed to understand the adherence energy in the peeling of very soft and dissipative materials.

AUTHOR INFORMATION

Corresponding Authors

*E-mail: julien.chopin@ufba.br.
*E-mail: matteo.ciccotti@espci.fr.

ORCID

Julien Chopin: 0000-0001-5105-4437
Costantino Creton: 0000-0002-0177-9680

DOI: 10.1021/acs.macromol.8b01374
Macromolecules 2018, 51, 8605−8610

Notes

The authors declare no competing financial interest.

REFERENCES

(1) Ferry, J. *Viscoelastic Properties of Polymers*; Wiley: New York, 1970; p 292.
(2) Gent, A. N.; Petrich, R. P. Adhesion of Viscoelastic Materials to Rigid Substrates. *Proc. R. Soc. London, Ser. A* **1969**, *310*, 433−448.
(3) Kaelble, D. H. Theory and Analysis of Peel Adhesion: Rate-Temperature Dependence of Viscoelastic Interlayers. *J. Colloid Sci.* **1964**, *19*, 413−424.
(4) Andrews, E.; Kinloch, A. Mechanics of elastomeric adhesion. *J. Polym. Sci., Polym. Symp.* **1974**, *46*, 1−14.
(5) Maugis, D. Subcritical crack growth, surface energy, fracture toughness, stick-slip and embrittlement. *J. Mater. Sci.* **1985**, *20*, 3041−3073.
(6) Mueller, H.; Knauss, W. G. Crack propagation in a linearly viscoelastic strip. *J. Appl. Mech.* **1971**, *38*, 483−488.
(7) Schapery, R. A theory of crack initiation and growth in viscoelastic media. Part I: Theoretical Development. *Int. J. Fract.* **1975**, *11*, 141−159.
(8) de Gennes, P.-G. Fracture of a Weakly Crosslinked Adhesive. *CR. Acad. Sci. II* **1988**, *307*, 1949−1953.
(9) Saulnier, F.; Ondarçuhu, T.; Aradian, A.; Raphaël, E. Adhesion between a viscoelastic material and a solid surface. *Macromolecules* **2004**, *37*, 1067−1075.
(10) Persson, B.; Brener, E. Crack propagation in viscoelastic solids. *Phys. Rev. E* **2005**, *71*, 036123.
(11) Barthel, E.; Frétigny, C. Adhesive contact of elastomers: effective adhesion energy and creep function. *J. Phys. D: Appl. Phys.* **2009**, *42*, 195302.
(12) Gent, A. N.; Schultz, J. Effect of Wetting Liquids on the Strength of Adhesion of Viscoelastic Material. *J. Adhes.* **1972**, *3*, 281−294.
(13) Maugis, D.; Barquins, M. Adhesion of Viscoelastic Materials to Rigid Substrates. *In: Allen KW, editor. Adhesion 12. London: Elsevier Applied Science* **1988**, *310*, 205.
(14) Gent, A. N. Adhesion and strength of viscoelastic solids. Is there a relationship between adhesion and bulk properties? *Langmuir* **1996**, *12*, 4492−4496.
(15) Cristiano, A.; Marcellan, A.; Keestra, B. J.; Steeman, P.; Creton, C. Fracture of model polyurethane elastomeric networks. *J. Polym. Sci., Part B: Polym. Phys.* **2011**, *49*, 355−367.
(16) Hui, C.-Y.; Jagota, A.; Bennison, S. J.; Londono, J. D. Crack blunting and the strength of soft elastic solids. *Proc. R. Soc. London, Ser. A* **2003**, *459*, 1489−1516.
(17) Creton, C.; Ciccotti, M. Fracture and adhesion of soft materials: a review. *Rep. Prog. Phys.* **2016**, *79*, 046601.
(18) Villey, R.; Creton, C.; Cortet, P.; Dalbe, M.; Jet, T.; Saintyves, B.; Santucci, S.; Vanel, L.; Yarusso, D.; Ciccotti, M. Rate dependent elastic hysteresis during the peeling of pressure sensitive adhesives. *Soft Matter* **2015**, *11*, 3480−3491.
(19) Kaelble, D. H. Theory and Analysis of Peel Adhesion: and Mechanics Mechanisms. *Trans. Soc. Rheol.* **1959**, *3*, 161−180.
(20) Kaelble, D. H. Theory and Analysis of Peel Adhesion: Bond Stresses and Distributions. *Trans. Soc. Rheol.* **1960**, *4*, 45−73.
(21) Urahama, Y. Effect of peel load on stringiness phenomena and peel speed of pressure-sensitive adhesive tape. *J. Adhes.* **1989**, *31*, 47−58.
(22) Chiche, A.; Dollhofer, J.; Creton, C. Cavity growth in soft adhesives. *Eur. Phys. J. E: Soft Matter Biol. Phys.* **2005**, *17*, 389−401.
(23) Benyahia, L.; Verdier, C.; Piau, J.-M. The mechanisms of peeling of uncross-linked pressure sensitive adhesives. *J. Adhes.* **1997**, *62*, 45−73.
(24) Gay, C.; Leibler, L. Theory of Tackiness. *Phys. Rev. Lett.* **1999**, *82*, 936−939.
(25) Derail, C.; Allal, A.; Marin, G.; Tordjeman, P. Relationship between Viscoelastic and Peeling Properties of Model Adhesives. Part 1. Cohesive Fracture. *J. Adhes.* **1997**, *61*, 123−157.
(26) Yarusso, D. J. Quantifying the Relationship Between Peel and Rheology for Pressure Sensitive Adhesives. *J. Adhes.* **1999**, *70*, 299−320.
(27) Cox, W. P.; Merz, E. H. Correlation of dynamic and steady flow viscosities. *J. Polym. Sci.* **1958**, *28*, 619−622.
(28) Kaelble, D. H. Theory and analysis of peel adhesion: adhesive thickness effects. *J. Adhes.* **1992**, *37*, 205−214.
(29) Deplace, F.; Rabjohns, M. A.; Yamaguchi, T.; Foster, A. B.; Carelli, C.; Lei, C.-H.; Ouzineb, K.; Keddie, J. L.; Lovell, P. A.; Creton, C. Deformation and adhesion of a periodic softsoft nanocomposite designed with structured polymer colloid particles. *Soft Matter* **2009**, *5*, 1440.
(30) Creton, C.; Hu, G.; Deplace, F.; Morgret, L.; Shull, K. R. Large-strain mechanical behavior of model block copolymer adhesives. *Macromolecules* **2009**, *42*, 7605−7615.
(31) Barrios, C. Anatomy of the deformation of pressure sensitive adhesives (PSAs) from rigid substrates. Proceedings of the Pressure Sensitive Tapes Council (PSTC) Tech 40, NV, May 17−19,2017.
(32) Sentmanat, M.; Wang, B. N.; McKinley, G. H. Measuring the transient extensional rheology of polyethylene melts using the SER universal testing platform. *J. Rheol.* **2005**, *49*, 585−606.
(33) Deplace, F.; Carelli, C.; Mariot, S.; Retsos, H.; Chateauminois, A.; Ouzineb, K.; Creton, C. Fine tuning the adhesive properties of a soft nanostructured adhesive with rheological measurements. *J. Adhes.* **2009**, *85*, 18−54.
(34) Wagner, M. A constitutive analysis of uniaxial elongational flow data of low-density polyethylene melt. *J. Non-Newtonian Fluid Mech.* **1978**, *4*, 39−55.
(35) Bird, R. B.; Armstrong, R. C.; Hassager, O. *Dynamics of Polymeric Liquids*; John Wiley and Sons Inc.: New York, 1987; Vol. *1*.
(36) Villey, R.; Cortet, P.-P.; Creton, C.; Ciccotti, M. In-situ measurement of the large strain response of the fibrillar debonding region during the steady peeling of pressure sensitive adhesives. *Int. J. Fract.* **2017**, *204*, 175−190.
(37) Cortet, P.-P.; Dalbe, M.-J.; Guerra, C.; Cohen, C.; Ciccotti, M.; Santucci, S.; Vanel, L. Intermittent stick-slip dynamics during the peeling of an adhesive tape from a roller. *Phys. Rev. E* **2013**, *87*, 022601.
(38) Chikina, I.; Gay, C. Cavitation in adhesives. *Phys. Rev. Lett.* **2000**, *85*, 4546.
(39) Gardon, J. L. Peel adhesion. I. Some phenomenological aspects of the test. *J. Appl. Polym. Sci.* **1963**, *7*, 625−641.
(40) Hata, T. Mechanisms of Adhesive Failure. *J. Adhes.* **1972**, *4*, 161−170.

DOI: 10.1021/acs.macromol.8b01374
Macromolecules 2018, 51, 8605−8610